



Contents lists available at ScienceDirect

Sensors and Actuators A: Physical

journal homepage: www.elsevier.com/locate/sna



Radial flow electroosmotic pump

Michael A. Schroeder^{a,1}, Kamil S. Salloum^{a,2}, Michel Perbost^b, Michal Lebl^{a,b}, Jonathan D. Posner^{a,*}

^a Mechanical Engineering, Chemical Engineering, Arizona State University, Tempe, AZ 85287, USA

^b Illumina Inc., San Diego, CA 92121, USA

ARTICLE INFO

Article history:

Received 19 October 2010

Received in revised form 19 April 2011

Accepted 12 May 2011

Available online xxx

Keywords:

Electroosmotic pump

Electroosmosis

Radial geometry

Semi-permeable membrane

Porous glass

ABSTRACT

This paper presents a radial frit geometry electroosmotic pump with a soft, semi-permeable gas venting membrane top. Radial pumps exhibit more than three times the average open flow rate per applied voltage and four times the average flow rate per sourced power than linear pumps for a given pump package volume. The radial pump can operate over a 16 h period with varying load.

© 2011 Elsevier B.V. All rights reserved.

1. Introduction

Microfluidic technologies have advanced the development of portable devices for medical diagnostics [1], reagent manipulation [2], and power generation [3,4]. At the lab scale, fluid delivery to such devices is often accomplished by pressure gradients via syringe pumps or pressurized gases. Handheld devices will require compact and reliable pumps. Micro-pumps can be designed to generate specific flow rates and pressures with reasonable power consumption in a small scale, which makes them well adapted for use in such devices. Recent micro-pump technologies include piezoelectric reciprocating displacement pumps, electrohydrodynamic pumps, and electroosmotic (EO) pumps [5].

EO pumps are attractive and versatile for a variety of applications due to the fact that they have no moving parts, can scale to a wide range of form factors, and can achieve high flow rates and pressures in a compact package relative to other dynamic micro-pumps [6]. EO pumps use an electroosmotic flow at the interface between a porous medium and an electrolyte. At the interface of a liquid and solid, ions from the solution migrate to shield the surface charges, forming an electric double layer (EDL). When an external electric field is applied, columbic forces act on the diffuse ions in

the EDL, causing bulk motion of the electrolyte through viscous drag [7,8].

EO pump applications include the cooling of microchips [9,10], drug delivery [11], point-of-care testing systems [12], and have proved useful in PEM fuel cell water management [13] and fuel delivery [14]. Performance attributes of interest depend on the application and include flow rate per unit input current/power, pumping power, and thermodynamic efficiency. In an effort to describe and increase output flow rates and pressures, several pumping solvents [15] and fabrication methods, such as packed capillaries [16] and photolithography [17,18], have been employed [5]. The flow rate of EO pumps, Q , scales linearly with the EDL's effective surface potential, termed the zeta potential, ζ [19]. The use of porous glass provides a cost effective and robust pumping medium because of its pore size and it exhibits large and stable values of ζ compared to other surfaces [20].

Long term stability and operation is a prominent challenge in the design of EO pumps. In particular, long term operation is impaired by the generation of electrolysis gases within the pump that can occlude the frit pores [19]. Various methods have been developed to deal with gas generation within an EO pump. One method involves separation of the electrodes from the hydraulic circuit in order to prevent electrolysis gases from occluding the frit pores and maintain a stable pH. Several techniques have been devised to achieve this, such as using an ion exchange membrane [21–23] or a gel salt bridge [24] between the electrodes and fluid. In our previous work, we demonstrated an orientation independent gas recombination design that uses Nafion-sheathed electrodes, a catalyst chamber, and an osmotic membrane to reform electrolysis gases back into

* Corresponding author.

E-mail address: Jonathan.Posner@asu.edu (J.D. Posner).

¹ Current address: Intel Corporation, Chandler, AZ 85226, USA.

² Current address: Intel Corporation, Hillsboro, OR 97124, USA.

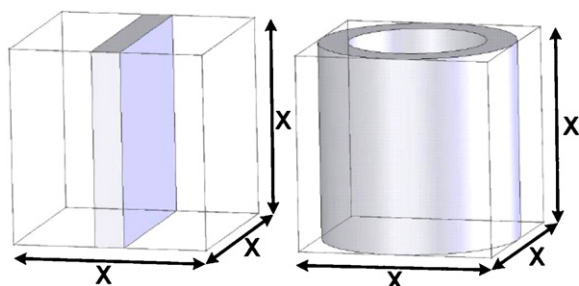


Fig. 1. Diagram showing a cube electroosmotic (EO) pump form factor, having dimensions X . The pumping medium of the cylindrical geometry has greater surface area, $\sim\pi X^2$, in comparison to the linear frit geometry, X^2 . The greater surface area will increase the output flow rate of the radial pump relative to the linear pump, for a constant effective voltage.

water [25]. Other designs for gas management have been developed that use alternating electric fields [26] or other periodic input signal schemes [27] that attempt to reduce the nucleation of electrolysis gases by reversing the polarity of the electrodes, and therefore dissolving gaseous species that have yet nucleated.

In this study, we present an EO pump that uses a radial frit pumping medium and a gas permeable membrane over the entire top of the pump housing to vent the electrolysis gases. Fig. 1 shows a comparison between linear and radial porous pumping medium geometries. In the same pump form factor, and for similar frit properties and thickness, the radial geometry increases the available surface area. We expect the increase in surface area to increase output flow rate for a fixed applied voltage as described by theoretical work in Yao and Santiago [28]. We also attempt to increase long term stability by sealing the entire top of the pump's housing with a gas permeable, liquid impermeable, membrane to vent the electrolysis gases generated within the pump. We characterize the radial EO pump's flow rate and pressure output at several galvanostatic and potentiostatic loads, and compare with a linear EO pump.

2. Experimental methodology

In this section we detail the design and construction of a radial EO pump as well as a linear EO pump that is used to test the relative performance. The experimental setup used to perform tests with the EO pump is also detailed.

2.1. Pump construction

We use ultrafine borosilicate sintered glass frits (D131766, Ace Glass Inc., Vineland, NJ) as the porous pumping medium. The glass frit surface properties are $0.55\ \mu\text{m}$ for the pore size, with a porosity of 0.24 and a tortuosity of 1.45 [19]. The frit's outer diameter, inner diameter, thickness, and height are 10 mm, 5 mm, 2.5 mm, and 10 mm respectively. The properties of the frit used in construction of the linear pump are identical to that of the radial frit with the exception of the frit geometry. The width and height of the square linear frit are 10 mm, with a thickness identical to the radial frit of 2.5 mm. The geometry of the frits is representative of the form factor presented in Fig. 1, where X in this case equals 10 mm.

The housing used is cylindrical with an open top and solid base, and is fabricated from machined polymethylmethacrylate (PMMA) plastic. The outer diameter of the housing is 21 mm, with a total height of 12 mm. To keep all geometric parameters between the linear and radial pumps identical with the exception of the frit surface area, the inner dimensions of the housings are set such that the total dead volume for each pump is 1.2 ml. The dead volume is the amount of liquid that resides in the pump during operation. We

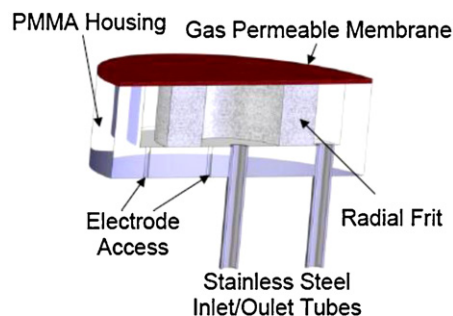


Fig. 2. Cross sectional diagram of the EO pump featuring radial frit geometry and gas permeable membrane.

use 0.127 mm wide platinum wire (SPPL-010, Omega Engineering, Stamford, CT) for the electrodes. The spacing between the electrodes is 3.5 mm for both the radial and linear pumps. Electrode spacing is ensured by accurate machining on the pump housing, where the electrodes are inserted and then fixed in place with epoxy. The inlet and outlet tubes are 0.125 inch outer diameter stainless steel (TUBN-125, Scanivalve Corp, Liberty Lake, WA). Fig. 2 shows a cross section view of the radial pump. All pump components were bonded together and sealed with quick set epoxy.

A Gore-Tex™ membrane (VE40814, Sealing Devices Inc., Lancaster, NY), permeable to gases and vapor and impermeable to liquid water, is adhered to the top of the pump housing to seal the frits and the enclosure. This membrane allows electrolysis gases to vent to the atmosphere but does not leak liquid water. We also pressurize liquid in the housing to aid the venting by placing the pump approximately 12 cm below the inlet and outlet reservoirs.

2.2. Experimental setup

Fig. 3 shows an overview of the experimental apparatus for testing the EO pumps. We connect the inlet reservoir, the EO pump, and the outlet reservoir in series with PTFE tubing. The outlet reservoir is placed on a mass balance (SI-603, Denver Instruments, Bohemia, NY) to record the gravimetric output of the pump. Mass balance data is collected via an RS232 port integrated with LabView. The flow rate is obtained through temporal differentiation of the mass balance data. We connect the electrodes of the EO pump to a sourcemeter (Model 2410, Keithley Instruments, Cleveland, OH) operating in either galvanostatic or potentiostatic mode. The sourcemeter is controlled with LabView via a general purpose interface bus (GPIB USB HS, National Instruments, Austin, TX).

For experiments involving pressure measurements, we use a pressure transducer (PX-303-015G5V, Omega Engineering, Stamford, CT) and micro-metering valve (P-445, Upchurch, Oak Harbor,

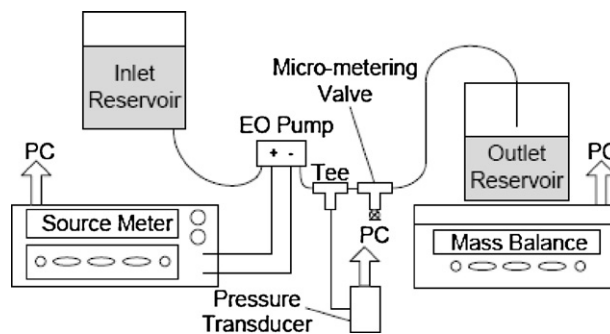


Fig. 3. Schematic of the experimental setup for flow rate, pressure, voltage and current measurements. Micro-metering valve, tee, and pressure transducer are only used when pressure measurements are made.

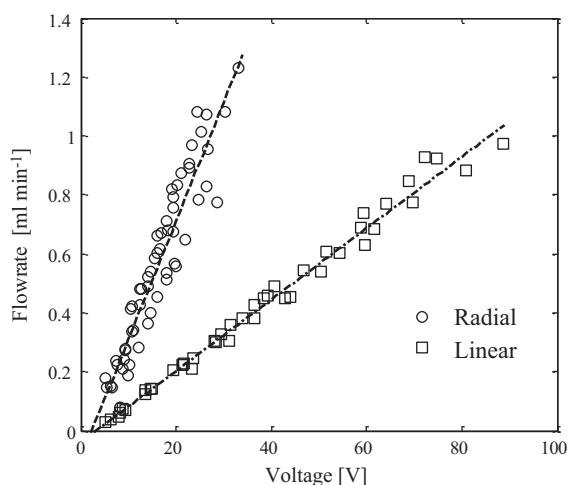


Fig. 4. Measured values of the average open flow rate as a function of the measured voltage for the linear (open squares) and radial (open circles) pumps operating under galvanostatic mode. The ratio of the slopes from the linear fits for each data set indicates that the radial flow rate is greater by a factor of ~ 3 .

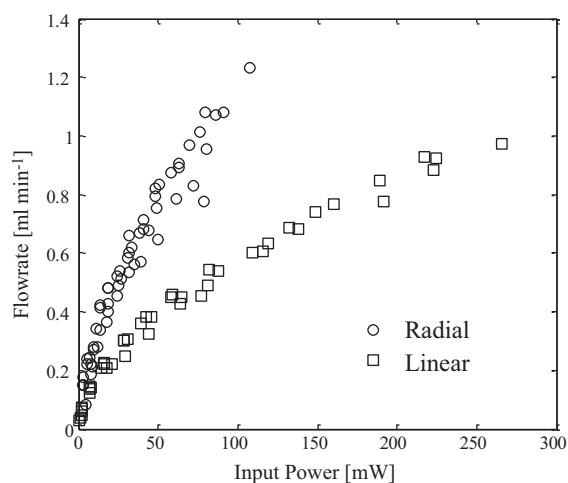


Fig. 5. Measured values of the maximum flow rate versus the input power for linear and radial pump configurations. As we increase the input power to the pump we observe larger flow rate outputs from the radial geometry.

WA) between the EO pump and outlet reservoir. The pressure data is collected from the transducer through a data acquisition card (NI-USB-6210, National Instruments, Austin Texas) and recorded in LabView. We use 0.125 inch outer diameter PTFE tubing for all fluidic connections, with the exception of connections between the transducer and micro-metering valve, which use 0.0625 inch outer diameter PTFE tubing.

For the working fluid, we use 1 mM sodium borate buffer to characterize the EO pump's output flow rates and pressures. The solution is prepared by dissolving sodium borate powder (part, Sigma-Aldrich, St. Louis, MO, USA) in 18.3 M Ω cm deionized water (Millipore, Billerica, MA) to a stock concentration of 0.2 M. The solution is then titrated with 0.2 M boric acid (B7901-500G, Sigma-Aldrich, St. Louis, MO) to a pH of 9, and then diluted to 1 mM.

2.3. Experimental procedure

Relationships for flow rate as functions of voltage and input power are obtained under galvanostatic conditions, where the applied current was varied from 0.25 to 3.25 mA in 0.25 mA increments. For each increment, the pump is run for 10 min. The reported flow rates and voltages are averaged over the duration of the run to obtain mean values for each increment of applied current. Between intervals, the pumps are mechanically flushed with a syringe using DI water.

Flow rate measurements as a function of pressure are obtained through incremental manipulation of back pressure with the use of the micro metering valve for potentiostatic and galvanostatic loads. The resulting pressure and flow rate for each increment are measured for a duration of 200 s. The flow rate and pressure are averaged over the duration of the measurement to obtain mean values.

3. Results and discussion

In this section, we present experimental results comparing the performance of the radial pump and linear pump. In particular, we examine flow rate in relation to voltage, input power, and pressure. We also compare our results with theoretical expectations.

3.1. Flow rate and pressure

Fig. 4 shows the average open flow rate (no pressure load) as a function of the voltage for the linear and radial pumps. Both of the flow rate and voltage values in Fig. 4 are measured and averaged from several galvanostatic runs on the linear and radial pumps. At any given voltage, the radial pump outputs approximately 3.32 times more flow rate than its linear counterpart. The flow rate's dependence on frit surface area can be inferred from theory [28], where the open flow rate is given by,

$$Q_{\max} = -\frac{\psi}{\tau} \frac{\epsilon f}{\mu} E_{\text{eff}} A, \quad (1)$$

where τ is the pore tortuosity, ψ is the frit porosity, ϵ is the solvent electrical permittivity, A is the frit area, E_{eff} is the electric field across the pumping medium, μ is the viscosity, and f is a dimensionless parameter (between 0 and 1) that is determined from a numerical solution of the Poisson-Boltzmann equation and depends on the pore size, buffer used, and the magnitude of the zeta potential [28]. To compare the expected flow rates between the linear and radial pumps for a given applied voltage, we compare the contributions from the area and the electric field in Eq. (1), where all the other terms are similar. The radial electric field is established as,

$$E_{\text{eff}} = \frac{V_{\text{eff}}}{\ln(r_2/r_1)r}, \quad (2)$$

where the electric field is a function of the radial distance r , such that $r_1 < r < r_2$, where r_1 and r_2 are the inner and outer frit radii respectively. The cylindrical surface area is defined as $A_r = 2\pi rX$, where X is the radial frit height. Computing the ratio of the radial and linear pumps' EA terms gives the relative flow rate performance.

$$\frac{Q_{\max-\text{rad}}}{Q_{\max-\text{lin}}} = \frac{90.65V_{\text{eff}}}{40V_{\text{eff}}} = 2.27 \quad (3)$$

We expect, given that all other properties are equivalent, that the radial pump's open flow rate will be 2.27 times larger than the linear geometry pump for a given applied voltage. The applied voltage can be approximated to be the effective voltage, as when the resistance loss from the electrode to the frit surface is considered in either geometrical configuration, we found the applied voltage is larger than 90% of the effective voltage [19]. Experimentally, we found that the open flow rate of the radial pump was 3.32 times greater than the linear pump, as computed by the ratio of the linear fits shown in Fig. 4 for a given applied voltage.

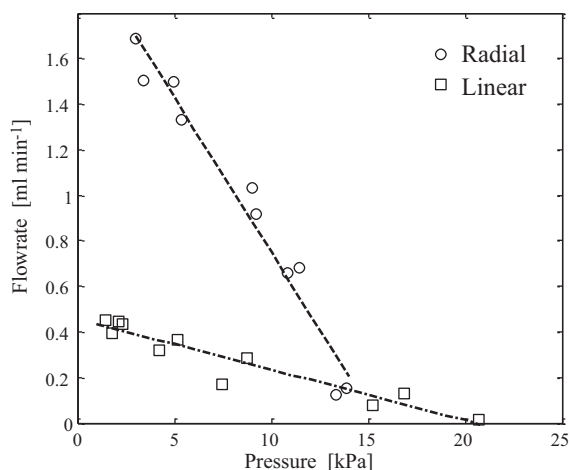


Fig. 6. Measured pressure versus the measured flow rate comparing the radial and linear pumps operated at a potentiostatic load of 45 V. The radial pump is expected to have 2.27 times larger relative Q_{\max} , and equivalent P_{\max} .

Fig. 5 shows the average open flow rate, for both radial and linear pumps, as a function of the input power, defined as the applied voltage multiplied by the sourced current. To sustain a required flow rate, the linear pump requires more input power than the radial pump. There is a nonlinear increase in the flow rate with input power from both pumps. This is expected since the flow rate is linear with voltage and the power scales as voltage squared. The difference in required input power also increases at higher flow rates, demanding substantial power input for the linear pump. For example, at a flow rate of 1 ml min^{-1} , the radial pump consumes roughly 4 times less power. Substantial increases in flow rate per applied power are achieved without compromising package size. Although radial geometry consumes less power in this operating condition, the overall efficiency of EO pumps is relatively low (<1%). The efficiency, given by the ratio of the pumping power to input power, at a flow rate of 1 ml min^{-1} for the linear and radial pump was approximately $1.5\text{e-}4$ and $3.25\text{e-}4$ respectively.

Fig. 6 presents flow rate as a function of the pressure for the radial and linear pumps under potentiostatic control. As we increase output pressure (through flow restriction), the pumps' flow rate decreases linearly similar to general pump behavior. Under potentiostatic loads, the radial and linear maximum pressure, ΔP_{\max} , should be equal. Theoretically, the maximum pressure, ΔP_{\max} , under constant voltage is given by

$$\Delta P_{\max} = -\frac{8\varepsilon\zeta V_{\text{eff}} f}{a^2} \quad (4)$$

where a is the frit pore diameter [28]. Fig. 6 shows that the maximum pressure for the radial pump is approximately 25% lower than the linear pump. At high pressures, the radial pump performance suffers due to detrimental changes in pH associated with electrolysis of the buffer, an issue that is discussed by Yao [19] and Brask [21]. Changes in pH associated with electrolysis are unfavorable because they result in lower zeta potential which lowers the maximum pressure [31]. This effect is exaggerated at low flow rates because there is insufficient advection to replenish the buffer [25]. The radial pump appears to suffer poignantly from these effects, attributed to pH gradients onset by electrolysis and concentration polarization inside the pump's small inner volume. The small dead volume of the radial pumps inner radius is only $200 \mu\text{l}$ (roughly 3 times smaller than the linear pump) and is subject to increased concentrations of acid relative to the outer dead volume, $1000 \mu\text{l}$, which contributes to pH polarization. Differences in V_{eff} may also contribute, despite that the same potential was applied to both pumps.

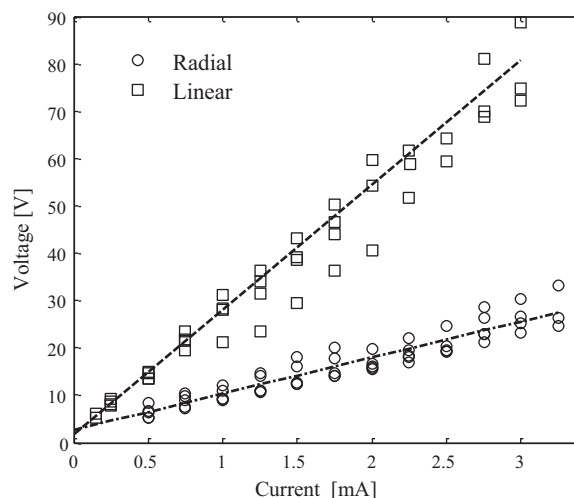


Fig. 7. Measured voltage as a function of the applied current shown for the radial and linear pumps. The radial pump displays π times less electrical resistance than the linear pump, which we attribute to differences in frit surface area.

Fig. 7 shows the voltage as a function of current for the linear and radial pump as measured under open flow rate conditions. The electrical resistances of the pumps are given by the slopes, where the linear pump has an electrical resistance that is larger than the radial pump by a factor of approximately 3. We attribute this to its larger frit area and equivalent porosity and buffer properties.

Fig. 8 shows the flow rate as a function of the pressure under galvanostatic control for the linear and radial pumps. The pumps have nearly equivalent maximum flow rates. Both pumps show a roughly linear decrease in flow rate with increasing back pressure. The linear pump exhibits a maximum pressure greater by a factor of seven times that of the radial pump.

Under galvanostatic control, the maximum flow rate is given as

$$Q_{\max} = -I_{\max} \frac{\varepsilon\zeta}{\mu\sigma_{\infty}} g, \quad (5)$$

where I is the applied current, σ_{∞} is the electrolyte conductivity, and g is a dimensionless flow rate per current ratio [28]. This equation clearly defines that the open flow rates are independent of the

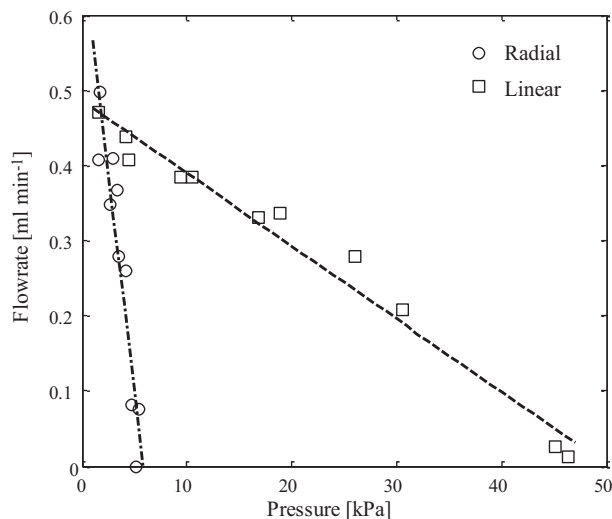


Fig. 8. Measured pressure versus the measured flow rate comparing the radial and linear pumps operated at a galvanostatic load of 1.5 mA. Based on theory, Q_{\max} is expected to be equivalent for the linear and radial pumps, which is reflected in the measured results. The linear pump exhibits a P_{\max} seven times greater than the radial pump.

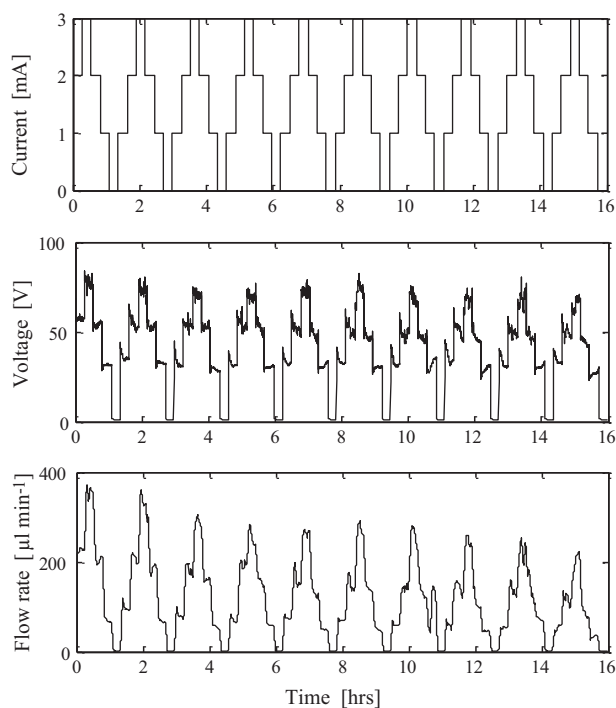


Fig. 9. The applied current, measured voltage, and measured flow rate are plotted as functions of time. The applied current is a square wave superimposed on a sinusoidal signal with a range of 0–3 mA, which was used to test the resilience and long term stability and response of the venting semi-permeable membrane equipped pump.

frit surface area as verified by our experiments shown in Fig. 8. To predict the maximum pressure of the linear pump relative to the radial pump under galvanostatic loads, Ohm's law is substituted in to Eq. (4), where V now becomes IR , effectively making the maximum pressure a function of the applied current. Using the relative electrical resistance (shown in Fig. 7), the maximum linear pump pressure can be approximated to be ~ 3 times greater relative to the radial pump for a given galvanostatic load. We attribute the difference between the predicted and measured maximum pressures to the limited internal dead volume of the radial pump. The radial pump suffers from detrimental changes in zeta potential due to pH degradation attributed to increased concentration of acid in the small inner dead volume. Degradation of pumping pressure at low flow rates has also been previously reported [18,32].

3.2. Long term operation

The semi-permeable membrane passively mitigates the effects of pump degradation due to electrolysis gases generated within the pump. Electrolysis gases can occlude the frit pores reducing the effective surface area. Equivalent pumps with a hard, non-venting top typically demonstrate low or no flow rate within 3 h of operation at moderate applied currents of 1–2 mA [30]. Fig. 9 shows the applied current, measured voltage and measured flow rate as functions of time over a duration of 16 h for a pump equipped with a semi-permeable top. The applied current ranged from 0 to 3 mA in 1 mA steps to simulate various working conditions. The radial pump demonstrates the ability to generate a flow rate over a long duration of time for a range of applied loads. The flow rate only decreases approximately 38% over the 16 h period based on the maximum flow rate given by the first and last peaks in the plot. Fig. 10 shows the measured flow rate for a duration of 6 h operating at a continuous applied current of 2 mA for another pump equipped with the semi-permeable top. The radial pump in Fig. 10

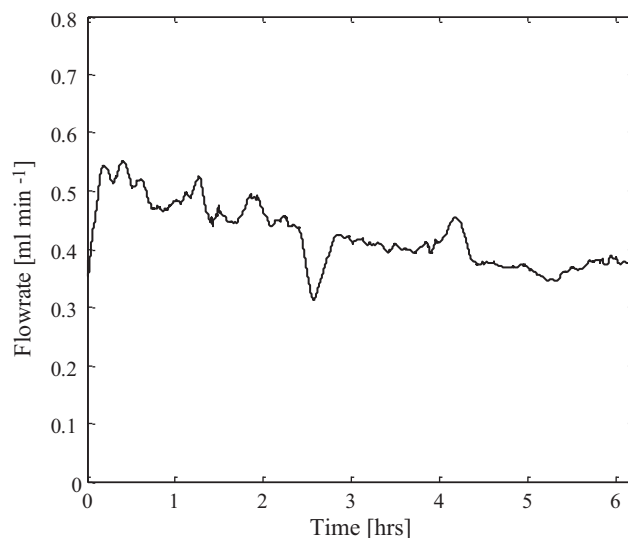


Fig. 10. Measured flow rate as a function of time for a radial pump with a semi-permeable membrane over a duration of 6 h at an applied current of 2 mA. Notably, the pump had been used for numerous tests, accumulating more than 50 h of operation and still demonstrated relatively good stability and only a 29% decrease in flow rate over the duration of the run.

had been used for numerous tests, accumulating more than 50 h of operation, and still demonstrated good stability.

4. Conclusion

We present an EO pump that utilizes radial frit geometry with a soft top, gas permeable membrane. For the same pump form factor and dead volume, radial frit geometry delivers a given flow rate with less input power than typical linear architecture, largely due to its greater frit surface area. The flow rate generated by the radial pump for a given applied voltage in our experiments was greater than the linear pump by a factor of ~ 3 . The radial pump generates lower maximum pressures than linear pump due to modifications in solvent pH in the small inner reservoir of the radial pump. Radial geometry offers large gas venting areas. Radial soft top EO pumps may find application in stationary instruments or instruments with defined orientation relative to gravity. Radial geometry also allows for the creation of multi-chamber arrangement of the pump [30,33].

Acknowledgement

This work was supported by Illumina Inc.

References

- [1] A.W. Martinez, S.T. Phillips, G.M. Whitesides, E. Carrilho, Diagnostics for the developing world: microfluidic paper-based analytical devices, *Anal. Chem.* 82 (3–10) (2010).
- [2] T. Thorsen, S.J. Maerkl, S.R. Quake, Microfluidic large-scale integration, *Science* 298 (2002) 580–584.
- [3] K.S. Salloum, J.R. Hayes, C.A. Friesen, J.D. Posner, Sequential flow membraneless microfluidic fuel cell with porous electrodes, *J. Power Sources* 180 (2008) 243–252.
- [4] E. Kjeang, N. Djilali, D. Sinton, Microfluidic fuel cells: a review, *J. Power Sources* 186 (2009) 353–369.
- [5] D.J. Laser, J.G. Santiago, A review of micropumps, *J. Micromech. Microeng.* 14 (2004) R35–R64.
- [6] X.Y. Wang, C. Cheng, S.L. Wang, S.R. Liu, Electroosmotic pumps and their applications in microfluidic systems, *Microfluid. Nanofluid.* 6 (2009) 145–162.
- [7] W. Sparreboom, A. van den Berg, J.C.T. Eijkel, Transport in nanofluidic systems: a review of theory and applications, *New J. Phys.* 12 (2010).
- [8] G.W. Slater, F. Tessier, K. Kopecka, The electroosmotic flow (EOF) in: micro-engineering in biotechnology, Humana Press Inc. (2010) 121–134.
- [9] L.N. Jiang, J. Mikkelsen, J.M. Koo, D. Huber, S.H. Yao, L. Zhang, P. Zhou, J.G. Maveety, R. Prasher, J.G. Santiago, T.W. Kenny, K.E. Goodson, Closed-loop elec-

trosmotic microchannel cooling system for VLSI circuits, IEEE Trans. Compon. Packag. Technol. 25 (2002) 347–355.

- [10] Y. Berrouche, Y. Avenas, C. Schaeffer, H.C. Chang, P. Wang, Design of a porous electroosmotic pump used in power electronic cooling, IEEE Trans. Ind. Appl. 45 (2009) 2073–2079.
- [11] L.X. Chen, J. Choo, B. Yan, The microfabricated electrokinetic pump: a potential promising drug delivery technique, Expert Opin. Drug Deliv. 4 (2007) 119–129.
- [12] A. Nisar, N. Aftulpurkar, B. Mahaisavariya, A. Tuantranont, MEMS-based micropumps in drug delivery and biomedical applications, Sens. Actuators B: Chem. 130 (2008) 917–942.
- [13] S. Litster, C.R. Buie, T. Fabian, J.K. Eaton, J.G. Santiago, Active water management for PEM fuel cells, J. Electrochem. Soc. 154 (2007) B1049–B1058.
- [14] C.R. Buie, D. Kim, S. Litster, J.G. Santiago, An electro-osmotic fuel pump for direct methanol fuel cells, Electrochem. Solid State Lett. 10 (2007) B196–B200.
- [15] D. Kim, J.D. Posner, J.G. Santiago, High flow rate per power electroosmotic pumping using low ion density solvents, Sens. Actuators A: Phys. 141 (2008) 201–212.
- [16] S.L. Zeng, C.H. Chen, J.G. Santiago, J.R. Chen, R.N. Zare, J.A. Tripp, F. Svec, J.M.J. Frechet, Electroosmotic flow pumps with polymer frits, Sens. Actuators B: Chem. 82 (2002) 209–212.
- [17] T.E. McKnight, C.T. Culbertson, S.C. Jacobson, J.M. Ramsey, Electroosmotically induced hydraulic pumping with integrated electrodes on microfluidic devices, Anal. Chem. 73 (2001) 4045–4049.
- [18] S.H. Yao, A.M. Myers, J.D. Posner, K.A. Rose, J.G. Santiago, Electroosmotic pumps fabricated from porous silicon membranes, J. Microelectromech. Syst. 15 (2006) 717–728.
- [19] S.H. Yao, D.E. Hertzog, S.L. Zeng, J.C. Mikkelsen, J.G. Santiago, Porous glass electroosmotic pumps: design and experiments, J. Colloid Interface Sci. 268 (2003) 143–153.
- [20] R. Venditti, X.C. Xuan, D.Q. Li, Experimental characterization of the temperature dependence of zeta potential and its effect on electroosmotic flow velocity in microchannels, Microfluid. Nanofluid. 2 (2006) 493–499.
- [21] A. Brask, J.P. Kutter, H. Bruus, Long-term stable electroosmotic pump with ion exchange membranes, Lab Chip 5 (2005) 730–738.
- [22] Y. Berrouche, Y. Avenas, C. Schaeffer, P. Wang, H.C. Chang, Optimization of high flow rate nanoporous electroosmotic pump, J. Fluids Eng. 130 (2008).
- [23] P. Wang, Z. Chen, H.C. Chang, An integrated micropump and electrospray emitter system based on porous silica monoliths, Electrophoresis 27 (2006) 3964–3970.
- [24] Y. Takamura, H. Onoda, H. Inokuchi, S. Adachi, A. Oki, Y. Horiike, Low-voltage electroosmosis pump for stand-alone microfluidics devices, Electrophoresis 24 (2003) 185–192.
- [25] C.W. Lin, S.H. Yao, J.D. Posner, A.M. Myers, J.G. Santiago, Toward orientation-independent design for gas recombination in closed-loop electroosmotic pumps, Sens. Actuators B: Chem. 128 (2007) 334–339.
- [26] A. Brask, D. Snakenborg, J.P. Kutter, H. Bruus, AC electroosmotic pump with bubble-free palladium electrodes and rectifying polymer membrane valves, Lab Chip 6 (2006) 280–288.
- [27] P. Selvaganapathy, Y.S.L. Ki, P. Renaud, C.H. Mastrangelo, Bubble-free electrokinetic pumping, J. Microelectromech. Syst. 11 (2002) 448–453.
- [28] S.H. Yao, J.G. Santiago, Porous glass electroosmotic pumps: theory, J. Colloid Interface Sci. 268 (2003) 133–142.
- [30] M.A. Schroeder, Radial Architecture Electroosmotic Pump Operational Characterization and Optimization in: Mechanical Engineering, Arizona State University, Tempe, 2010, p. 70.
- [31] B.J. Kirby, E.F. Hasselbrink, Zeta potential of microfluidic substrates: 1. Theory, experimental techniques, and effects on separations, Electrophoresis 25 (2004) 187–202.
- [32] M.E. Suss, A. Mani, T.A. Zangle, J.G. Santiago, Electroosmotic pump performance is affected by concentration polarizations of both electrodes and pump, Sens. Actuators A: Phys. 165 (2011) 310–315.
- [33] J. Posner, K. Salloum, M. Lebl, M. Reed, D. Buermann, M. Hage, B. Crane, D. Heiner, R. Kain, Electroosmotic Pump with Improved Gas Management, WIPO, 2010.

Biographies



Michael Schroeder earned his BS and MS degrees in mechanical engineering from Arizona State University. As a graduate student and research assistant working in the microfluidics lab, his work included electroosmotic pumps for DNA sequencing applications. Currently he is employed at Intel, where he works in the thermal fluids lab as a packaging engineering in the Core Competency division of the Assembly & Test Technology Development group.



Kamil Salloum received his BSE and PhD degrees from Arizona State University in 2006 and 2010. His doctoral research focused on the development and characterization of membraneless microfluidic fuel cells. He has published experimental work on novel microfluidic flow fields for membraneless fuel cells, including the use of porous electrodes and reactant separation and recycling. He also worked on developing a high flow rate per input power electroosmotic pump for biotech applications. Throughout his graduate career he has accumulated five patent applications, four in the field of microfluidic fuel cells and one in electroosmotic pumping. Kamil is currently employed as a process technology development engineer at Intel's Logic Technology Development (LTD) division in Hillsboro Oregon.



Michel Perbost, nucleic acid chemist, got his PhD in Montpellier, France in 1992. After a postdoc at Isis pharmaceuticals developing novel antisense molecules, he worked 6 years at Agilent as part of the team that created the DNA array business. He moved to Connecticut working at Molecular Staging on Protein arrays. In 2004 he worked at CyVera, a startup biotech, developing a novel bead assay platform, which was acquired in 2005 by Illumina, a San Diego biotech, world leader in DNA arrays and DNA sequencing. Two years later, Michel Perbost transferred CyVera technologies to San Diego, upgrading the processes and production equipments. He works now in the Research department developing novel instruments.



Michal Lebl obtained his Ph.D. from the Institute of Organic Chemistry and Biochemistry of the Czechoslovak Academy of Sciences in Prague in 1978 (D.Sc. in 1992). In 1991 he moved to USA and worked as Director of Chemistry in Selectide Corporation, the first combinatorial chemistry company in the world, in Tucson. In 1993 he formed Spyder Instruments, which in 2000 merged with the new startup biotech company Illumina Inc., which became the leading genomics company in the world. Dr. Lebl works at Illumina, Inc. as Senior Director since then. Dr. Lebl is the recipient of several awards, the most prestigious being the Leonidas Zervas Award of the European Peptide Society and the 2003 Jouan Award for his contributions to laboratory automation and laboratory process improvement. He is a member of the editorial boards of scientific journals, and serves on the scientific advisory boards of several companies.



Jonathan D. Posner is an associate professor at Arizona State University in the faculties of Mechanical Engineering and Chemical Engineering as well as adjunct faculty in the Consortium for Science, Policy, & Outcomes (CSPO). Dr. Posner earned his Ph.D. (2001) degree in Mechanical Engineering at the University of California, Irvine. He spent 18 months as a fellow at the von Karman Institute for Fluid Mechanics in Rhode Saint Genèse, Belgium and two years as a postdoctoral fellow at the Stanford University. His interests include electrokinetics, micro/nanofluidics, electrochemistry, self-assembly of colloids, and the physics of nanoparticles at interfaces. At CSPO, Posner has interest in the social implications of technology, role of science in policy and regulation, as well as ethics education. Dr. Posner was honored with a 2008 NSF CAREER award for his work on the physics of self-assembly of nanoparticles at fluid-solid and fluid-fluid interfaces. He has also been recognized for his Excellence in Experimental Research by the von Karman Institute for Fluid Dynamics.